A sub-pixel level map projection conversion method for high resolution of GF3 satellite products

Wentao Wang, Jiayin Liu, Lijia Huang
Key Laboratory of Technology on Geo-spatial Information Processing and Application System, Institute of Electronics, Chinese Academy of Sciences, University of Chinese Academy of Sciences
Beijing , China
Email:wangwentao16@mails.ucas.ac.cn ,liujy@mail.ie.ac.cn, iecas8huanglijia@163.com

Abstract

The GF-3 satellite launched in August 2016, is a C-band synthetic aperture radar(SAR) in China. With a resolution up to 1 m, GF-3 SAR imagery have made feasible the generation large-scale high resolution maps which need a high precision image registration technique. However, different remote sensing data usually have different geocoded formats. It causes misregistration when register SAR image with different projection formats. This paper discusses the method that convert the images from various projection coordinate to the unified geographic coordinate with a conversion accuracy of sub-pixel level.

1 Introduction

The GF-3 satellite launched in August 2016, is a C-band multi-polarization synthetic aperture radar in China. It has 12 imaging modes which is the largest number of imaging modes of any SAR satellite in the world. With the abilities of working all-weather and all-day, GF-3 satellite will play a significant role in land and ocean monitoring, catastrophic weather warning, natural resources accessing.

SAR image registration has a widely use in image fusion, image mosaic and image classification. As the basis of SAR image post-processing, the precision of registration has a great impact on SAR image applications. Since the images used in the registration are acquired from different SAR sensors or different types of sensors, these images usually have different geocoded formats which contributes to the difficulty in registration. A convenient way is to convert the projection coordinate to the unified geographic coordinate. In this study, a conversion methed that converting the projection coordinate to geographic coordinate is realized by using GF-3 level 2 data. Test results show that the conversion accuracy is within one pixel, though realizing a sub-pixel level map projection.

2 Products

The basic GF-3 image products include three level products: level 0, level 1, level 2. Level 0 product is raw data. Level 1 product contains level 1a and level 1b data and it provides metadata, incidence data, auxiliary data at the same time. Level 2 product contains the coarse geocoded image using average terrain height.

3 Inverse map projection conversion method

Since there are many map projection formats, this section provides a brief description of the inverse map projection process. An example is illustrated converting the Universal Transverse Mercator (UTM) projection coordinate to the geographic coordinate. The inverse map projection conversion method is splited into two main parts illustrated in the following:

3.1 Inverse map projection

The UTM projection is an elliptical cylindrical projection with an equal angle transverse axis. The center line of the elliptical cylinder is located on the equatorial plane of the ellipsoid, and through the ellipsoid body point. The points on the ellipsoid are projected onto the elliptic cylinder and the length of the two secant circles has no change on the UTM projection graph. In this paper, the UTM projection we used is based on WGS-84 earth ellipsoid and the ellipsoid is partitioned into 60 zones of 6° longitude where the central meridian is in the center of each zone. The central meridian is mapped onto the plane with a scale factor of 0.9996 and represents the y-axis. The x-axis is the mapping of the equator.

For the inverse UTM projection, a point (y, x)in the plane being mapped into a point (φ , λ)on the ellipsoid is given by the series expansions:

$$\begin{aligned}\varphi=&\varphi_f+\frac{t_f}{2N_f^2}(-1-\eta_f^2)x^2\\&+\frac{t_f}{24N_f^4}(5+3t_f^2+6\eta_f^2-6t_f^2\eta_f^2-3\eta_f^4-9t_f^2\eta_f^4)x^4\\&+\frac{t_f}{720N_f^6}(-61-90t_f^2-45t_f^4-107\eta_f^2+162t_f^2\eta_f^2+45t_f^4\eta_f^2)x^6\\&+\frac{t_f}{40320N_f^8}(1385+3633t_f^2+4095t_f^4+1575t_f^8)x^8+...\end{aligned} \tag{1}$$

$$\begin{aligned}\lambda=&\lambda_0+\frac{1}{N_f\cos\varphi_f}x+\frac{1}{6N_f^3\cos\varphi_f}(-1-2t_f^2-\eta_f^2)x^3\\&+\frac{1}{120N_f^5\cos\varphi_f}(5+28t_f^2+24t_f^4+6\eta_f^2+8t_f^2\eta_f^2)x^5\\&+\frac{1}{5040N_f^7\cos\varphi_f}(-61-662t_f^2-1320t_f^4-720t_f^6)x^7+...\end{aligned} \tag{2}$$

where

$$\begin{aligned}e'^2&=(a^2-b^2)/b^2\\\eta_f&=e'^2\cos^2\varphi_f\\t_f&=\tan\varphi_f\\N_f&=\frac{a^2}{b^2\sqrt{1+\eta^2}}\end{aligned} \tag{3}$$

the terms with the subscript f must be calculated based on the footpoint latitude φ_f, which can be computed by the series expansion

$$\varphi_f=\bar{y}+\bar{\beta}\sin 2\bar{y}+\bar{\gamma}\sin 4\bar{y}+\bar{\delta}\sin 6\bar{y}+\bar{\varepsilon}\sin 8\bar{y}+... \tag{4}$$

where

$$\begin{aligned}\bar{\alpha}&=\frac{a+b}{2}(1+\frac{1}{4}n^2+\frac{1}{64}n^4+...)\\\bar{\beta}&=\frac{3}{2}n-\frac{27}{32}n^3+\frac{269}{512}n^5+...\\\bar{\gamma}&=\frac{21}{16}n^2-\frac{55}{22}n^4+...\\\bar{\delta}&=\frac{151}{96}n^2-\frac{417}{128}n^5+...\\\bar{\varepsilon}&=\frac{1097}{512}n^4+...\\\bar{y}&=\frac{y}{\bar{\alpha}}\end{aligned} \tag{5}$$

In our examples, the parameters for WGS-84 ellipsoid are computed in the **Table 1**:

Table 1: Parameters for WGS-84 ellipsoid

Parameter	WGS-84 ellipsoid
$\bar{\alpha}$	$6367449.1458m$
$\bar{\beta}$	$2.51882658\cdot10^{-3}$
$\bar{\gamma}$	$3.70095\cdot10^{-6}$
$\bar{\delta}$	$7.45\cdot10^{-9}$
$\bar{\varepsilon}$	$17\cdot10^{-12}$

In practical use, the central meridian of each zone is defined to coincide with 500000 meters East avoiding dealing with negative numbers. Similarly, positions are measured northward from zero at the equator in the northern hemisphere and the equatorial coordinate value is set at 10000000 in the southern hemisphere. Thus, the point value (y, x) in formula (1) (2) need to be adjusted by the formula (6)：

$$\begin{aligned}x&=\frac{x-500000}{0.9996}\\y&=\begin{cases}\dfrac{y}{0.9996}, northern\ hemisphere\\\dfrac{y-10000000}{0.9996}, southern\ hemisphere\end{cases}\end{aligned} \tag{6}$$

It can be proved by experiments that this method used to inverse mapping can achieve a millimeter accuracy.

3.2 Resample

There many methods in image resampling: the nearest neighbor method, bilinear interpolation method, bi-cubic convolution method. Taking the effect of resampling and the running time into account, we choose bilinear interpolation method in this experiment.

Bilinear Interpolation computes a weighted average of the four nearest cell centers as the value of the input cell center. A closer distant from an input cell center to output cell center will have a higher effect on the value of the output cell value. This means the output cell value could not be the same as the nearest cell input, but always has the same range of values as the input. The main idea of the bilinear interpolation method is to perform linear interpolation in two directions respectively and the interpolation formula (7) is illustrated by **Figure 1**.

$$\begin{aligned}P&=W_{11}R_{11}+W_{12}R_{12}+W_{21}R_{21}+W_{22}R_{22}\\&=(1-\Delta x)(1-\Delta y)R_{11}+(1-\Delta x)\Delta y R_{12}+\Delta x(1-\Delta y)R_{21}+\Delta x\Delta y R_{22}\end{aligned} \tag{7}$$

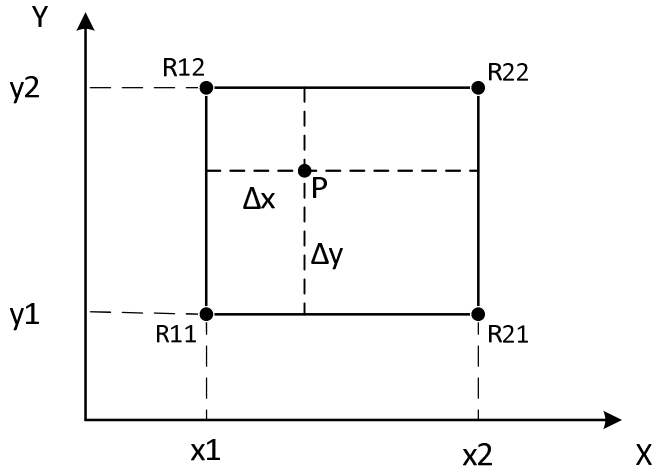

Figure 1: Schematic diagram of bilinear interpolation formula

The whole inverse map projection process can be shown as in **Figure 2**. Firstly, the geographic coordinates of four

corner points in geographic image can be calculated using UTM image in order to get the length and width of the geographic image. Then, for each pixel (i, j) in geographic pixel image, the corresponding mapping coordinates in UTM pixel image would be computed by the mapping relation G->F->T. Finally, each pixel value in geographic pixel image is determined by corresponding UTM image pixel using bilinear interpolation method.

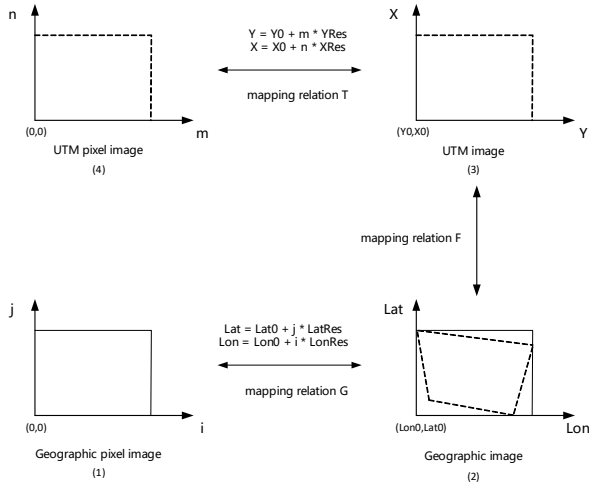

Figure 2: The flow of the inverse map projection

4 Experiment and Results

In this section, we conducted experiments to validate the accuracy of the inverse map projection. The investigated test site includes a small area of New Delhi, India. The used image data taken in September 6, 2017 is a high resolution spotlight GF-3 SAR level 2 image with a resolution of 1m. The size of the image is 13640 * 13485 and its map projection is UTM. **Figure 3** show the image of the test area.

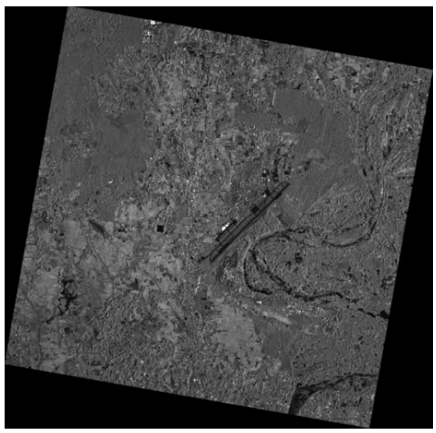

Figure 3: GF-3 SAR image: UTM projection coordinate

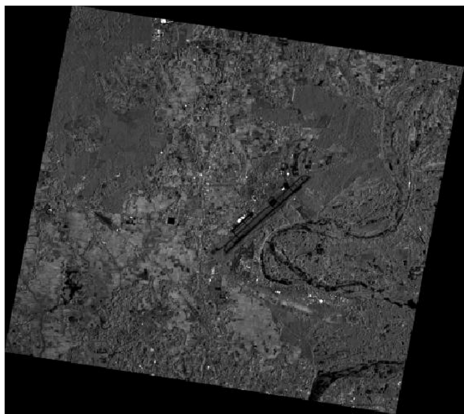

Figure 4: Conversion image: geographic coordinate

The commercial image analysis software ERDAS IMAGING 2013 is uesd to view and compare the two image. **Figure 4** show the result image of geographic coordinate computed by the inverse map projection method. **Figure 5** show the surveyed locations and its corresponding position in both scene using the geo-link function of ERDAS that can automatically locate the same position in the corresponding scene. The white cross represents the same position in the both scene. In each case, the compared scenes are at three zoom levels. The zoom level increases toward the bottom and the last zoom level is at pixel level. The first scene has UTM projection coordinate and the second scene has geographic coordinate in each case.

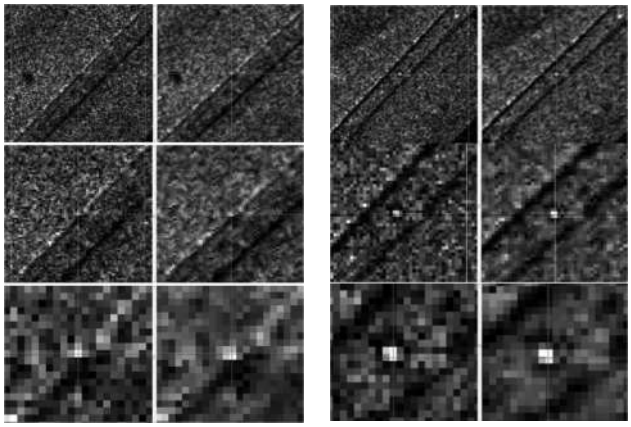

Figure 5: Two cases of comparison of the conversion result in the corresponding scenes. The first scene is UTM and the second scene is geographic in each case.

In further comparison, we selected a certain number of test points evenly in the image to test the conversion accuracy of the whole image. This is illustrated in **Figure 6**.

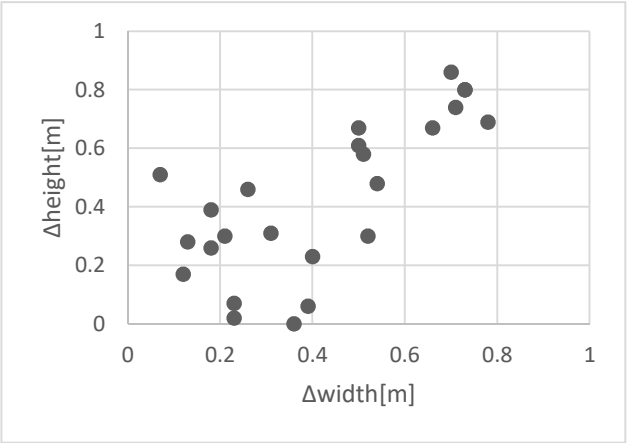

Figure 6: Projection accuracy of 24 test points evenly distributed in the whole image

From the test result above, it is clearly that the conversion accuracy of the inverse map projection method is within one pixel.

5 Conclusion

In this study, a method is described for inverse map projection conversion using GF-3 high resolution SAR image. It convert the images with different projection formats to the unified geographic coordinate with an accuracy of sub-pixel level solving the problem that register images acquired from different SAR sensors or different types of sensors.

6 Acknowledgment

This work is supported by the The Key Standard Technologies of National High Resolution Special (No.30-Y20A12-9004-15/16, No.03-Y20A11-9001-15/16 and No.41-Y20A13-9001-15/16).

7 References

[1] Wang H, Yang J, Mouche A, et al. GF-3 SAR Ocean Wind Retrieval: The First View and Preliminary Assessment[J]. Remote Sensing, 2017, 9(7):694.

[2] Ding C, Liu J,Lei B, et al.Preliminary exploration of systematic geolocation accuracy of GF-3 SAR satellite system. J. Radars 2017, 6, 11–16.

[3] Zhao R, Zhang G, Deng M, et al. Geometric Calibration and Accuracy Verification of the GF-3 Satellite[J]. Sensors, 2017, 17(9):1977.

[4] Xian-Chuan Y U, Zhong-Hua L, Dan H U. Review of remote sensing image registration techniques[J]. Optics & Precision Engineering, 2013, 21(11):2960-2972.

[5] Shao W, Sheng Y, Sun J. Preliminary Assessment of Wind and Wave Retrieval from Chinese Gaofen-3 SAR Imagery[J]. Sensors, 2017, 17(8).

[6] Hoffmann-Wellenhof B, Lichtenegger H, Collins J. GPS: Theory and Practice, 3rd ed. New York: Springer-Verlag Wien, 1994

[7] Curlander J C, Mcdonough R N. Synthetic Aperture Radar: Systems and Signal Processing[M]. John Wiley & Sons, 1991